Geophysical Research Letters

RESEARCH LETTER
10.1029/2019GL082456

Key Points:
- The propagation of infrasonic waves through the turbulence induced by the breaking of mountain waves is investigated numerically
- The numerical model is based on the 2-D Navier-Stokes equations
- The influence of small-scale turbulent fluctuations on infrasonic ground recordings is analyzed

Supporting Information:
- Supporting Information S1
- Movie S1
- Movie S2

Correspondence to:
R. Sabatini,
sabatinr@erau.edu;
roberto87sabatini@gmail.com

Citation:
Sabatini, R., Snively, J. B., Bailly, C., Hickey, M. P., & Garrison, J. L. (2019). Numerical modeling of the propagation of infrasonic acoustic waves through the turbulent field generated by the breaking of mountain gravity waves. *Geophysical Research Letters*, *46*, 5526–5534. https://doi.org/10.1029/2019GL082456

Received 13 FEB 2019
Accepted 13 APR 2019
Accepted article online 18 APR 2019
Published online 21 MAY 2019

Numerical Modeling of the Propagation of Infrasonic Acoustic Waves Through the Turbulent Field Generated by the Breaking of Mountain Gravity Waves

R. Sabatini[1], J. B. Snively[1], C. Bailly[2], M. P. Hickey[1], and J. L. Garrison[3]

[1]Center for Space and Atmospheric Research (CSAR) and Department of Physical Sciences, Embry-Riddle Aeronautical University, Daytona Beach, FL, USA, [2]Laboratoire de Mécanique des Fluides et dAcoustique, Unité mixte de recherche CNRS 5509, École Centrale de Lyon, Écully cedex, France, [3]School of Aeronautics and Astronautics, Purdue University, West Lafayette, IN, USA

Abstract The nonlinear propagation of low-frequency acoustic waves through the turbulent fluctuations induced by breaking mountain gravity waves is investigated via 2-D numerical simulations of the Navier-Stokes equations, to understand the effects of atmospheric dynamics on ground-based infrasound measurements. Emphasis is placed on acoustic signals of frequency around 0.1 Hz, traveling through tens-of-kilometers-scale gravity waves and subkilometer-scale turbulence. The sensitivity of the infrasonic phases to small-scale fluctuations is found to depend on the altitudes through which they are refracted toward the Earth. For the considered cases, the dynamics in the stratosphere impact the refracting acoustic waves to a greater extent than those in the thermosphere. This work clearly demonstrates the need for accurate descriptions of the effects of atmospheric dynamics on acoustic propagation, such as here captured by the full set of fluid dynamic equations, as well as of the subsequent effects on measured signals.

Plain Language Summary Infrasound is the low-frequency part of the acoustic spectrum, with periods ranging from around 0.05 s to about 300 s. Infrasonic waves are generated by a large variety of natural and artificial sources (such as earthquakes, volcanic eruptions, auroras, thunderstorms, explosions, rocket launches, and sonic booms) and can propagate up to the thermosphere and over thousands of kilometers on the ground. The ground recordings are currently employed in numerous applications, including the detection and localization of specific sources (such as clandestine nuclear tests) as well as the research in the domain of the atmospheric dynamics. Mountain gravity waves are buoyant motions associated with the gravitational acceleration and are excited as air flows over mountain ranges. They can have horizontal wavelengths as small as 10 km and as high as 100 km and, if sufficiently strong, can break and lead to smaller-scale turbulence. The subsequent turbulent fluctuations can severely influence the infrasonic waves. This paper reports the results of numerical simulations of the atmospheric propagation of infrasonic signals through the inhomogeneities induced by the breaking of mountain waves. The present analysis provides new insights into the understanding of the effects of the aforementioned turbulent perturbations on the infrasonic signals potentially recorded on the Earth's surface.

1. Introduction

Infrasonic acoustic waves (IAWs) of frequency f in the band $0.003 \lesssim f \lesssim 20$ Hz are generated in the Earth's atmosphere either by natural phenomena, such as earthquakes (Mutschlecner & Whitaker, 2005), volcanic eruption (Matoza et al., 2009), auroras (de Larquier et al., 2010), thunderstorms (Assink et al., 2008), and atmospheric entry of meteoroids (Gainville et al., 2017), or by anthropogenic sources, like aboveground and underground explosions (Assink et al., 2016; Ceranna et al., 2009; Yang et al., 2012; McKisic, 1997), rocket launches, and sonic booms (Le Pichon et al., 2002). As a result of the ducts resulting from the large-scale variations with altitude of the atmospheric temperature and winds, they travel up to the thermosphere and over thousands of kilometers horizontally (Drob et al., 2003) and carry important information about both their sources and their medium of propagation.

In addition to the vertical large-scale gradients of atmospheric properties, which are largely controlled by the solar radiative heating, large-scale waves, and tides and by gravity waves (GWs) and their momentum forcing, localized small-scale turbulent perturbations are also ubiquitous in the Earth's atmosphere (Bossert et al., 2015; Fritts & Alexander, 2003; Fritts et al., 2018; Hecht et al., 1997; Tsuda, 2014). Such fluctuations not only are responsible for partial reflections and scattering of the IAW signals (Chunchuzov et al., 2011, 2013, 2014, 2015) but can also amplify or weaken the various acoustic waveguides and in particular the stratospheric duct (Bertin et al., 2014; Lalande & Waxler, 2016). One of their most important causes is the breaking of GWs. GWs can be excited by multiple sources (Fritts & Alexander, 2003). As an example, orographic GWs, also called mountain waves (MWs), develop due to air flow over mountain ranges and exhibit horizontal scales as small as 10 km and as high as hundreds of kilometers, potentially at large amplitude (Bossert et al., 2015; Fritts et al., 2018). Orographic forcing is also likely to generate IAWs, which have been hypothesized to contribute to the heating of the thermosphere as they dissipate (Hickey et al., 2001; Walterscheid & Hickey, 2005).

Understanding the interaction between acoustic waves and turbulence is crucial to advance the science and applications of atmospheric infrasound. Recent sensitivity analyses (Bertin et al., 2014; Lalande & Waxler, 2016) have revealed that even small-amplitude perturbations of the atmospheric temperature and winds can severely affect the infrasonic signals recorded at ground level far from their source. Given the lack of knowledge of the ever-changing middle atmosphere, the strong sensitivity of the IAWs to the turbulent fluctuations raises a fundamental question of predictability. Investigating the interaction between the IAWs and the small-scale inhomogeneities is challenging. Although a number of studies have been carried out for applications near the ground (e.g., Ostashev & Wilson, 2016, and references therein) or to analyze the effect of temperature and wind fluctuations on sonic boom signatures (e.g., Luquet et al., 2015, and references therein), only few investigations have been performed on the long-range propagation of infrasound through GWs and their induced turbulence (Chunchuzov et al., 2011, 2013, 2014, 2015; Hedlin & Drob, 2014; Kulichkov, 2009; Lalande & Waxler, 2016). From a modeling perspective, great difficulty arises in the specification of the propagation medium (Lalande & Waxler, 2016), which is typically obtained from numerical weather predictions or from empirical and semiempirical models (Drob et al., 2003, 2008; Picone et al., 2002). Since the data thereby provided do not include small-scale structures, the unresolved dynamics of atmospheric GWs have been represented in recent infrasound studies as noise superimposed on the resolved mean state (Chunchuzov et al., 2015; Hedlin & Drob, 2014; Lalande & Waxler, 2016; Norris et al., 2009) and with specific spectral characteristics (Chunchuzov, 2009; Drob et al., 2013; Gardner, 1994).

Apart from this specification issue, comprehensive investigations of the interaction between IAW and the GW-induced turbulence have also been hampered by the inherent limitations of the propagation models employed in the framework of atmospheric acoustics, such as ray tracing, normal modes, and parabolic-equation methods, which do not incorporate all of the relevant physics.

In the last three decades, numerous studies on the propagation and breaking of GWs generated by different sources have been conducted by performing 2-D and 3-D simulations of the Navier-Stokes equations (e.g., Fritts & Alexander, 2003; Snively & Pasko, 2008, and references therein). The use of the full set of the fluid dynamic equations to investigate the 2-D and 3-D propagation of IAWs is a relatively recent subject of research, made feasible by advances of computational capabilities (de Groot-Hedlin, 2012, 2016, 2017; Marsden et al., 2014; Sabatini et al., 2016, 2019; Zettergren & Snively, 2015, 2019). In this work, the propagation of an IAW through the small-scale inhomogeneities induced by the breaking of a MW is analyzed by direct numerical simulations of the 2-D Navier-Stokes equations. The emphasis is here placed on an impulsive IAW generated on the Earth's surface, with a central frequency equal to about 0.1 Hz and with a wavelength of the order of 3.4 km near the ground. This choice is particularly relevant for explosive sources, which have received renewed attention in the framework of the Comprehensive Nuclear-Test-Ban Treaty (Le Pichon et al., 2009).

The purpose of the present study is twofold. First, the feasibility of simultaneously investigating the evolution of the atmospheric nonlinear wave dynamics and turbulence with the propagation of acoustic waves therein is demonstrated, for the first time in the framework of infrasonic acoustics. Second, a qualitative analysis of the effects of small-scale turbulent fluctuations on ground recordings is carried out, to provide a preliminary and nonexhaustive answer to the fundamental question of predictability of infrasonic arrivals. This demonstrates and motivates a pathway toward more comprehensive and quantitative 3-D investigations

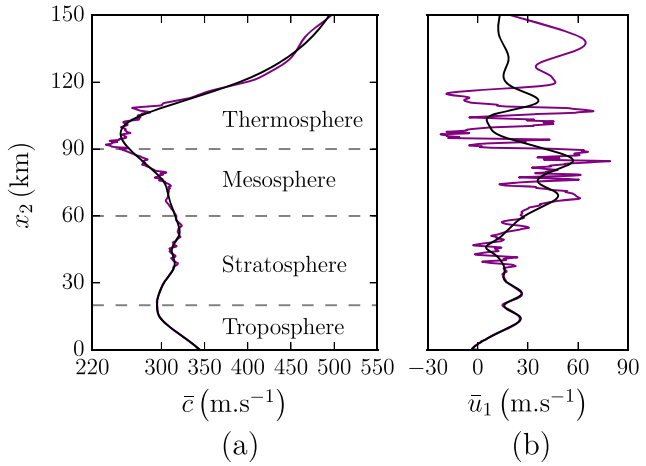

Figure 1. (a) Speed of sound $\bar{c}(x_2)$ and (b) horizontal wind $\bar{u}_1(x_2)$ of the initial unperturbed atmosphere for the first two configurations (black line) and for the NLP case (purple line).

of the interactions between IAWs and turbulent atmospheric dynamics (including both 2-D and 3-D cascades, as well as oblique propagation of IAWs and GWs) and of the subsequent effects on signals recorded at the ground, in the stratosphere (Bowman & Lees, 2015), or in the thermosphere-ionosphere (Zettergren & Snively, 2019).

The paper is organized as follows: In section 2, the model setup, the excitation of the MW and of the IAW, the initial atmospheric state, and the parameters of the different simulations are described; in section 3, the corresponding results are presented; concluding remarks are finally drawn in section 4.

2. Problem Definition and Case Studies

A Cartesian coordinate system with origin at ground level, horizontal axis x_1, and vertical axis x_2 is employed. The domain of interest ranges from $x_1 = 0\,\mathrm{km}$ to $x_1 = 800\,\mathrm{km}$ and from the ground at $x_2 = 0\,\mathrm{km}$ to $x_2 = 150\,\mathrm{km}$ altitude. The atmosphere is assumed to behave as a single ideal gas satisfying the equation of state $p = \rho RT$, where p is the pressure, ρ is the fluid density, T is the temperature, and $R = 287.06\,\mathrm{J{\cdot}kg^{-1}{\cdot}K^{-1}}$ is the specific gas constant. The speed of sound c is given by the relation $c = \sqrt{\gamma RT}$, where $\gamma = 1.4$ represents the ratio of specific heats. The fluid flow is described by the conservative variables $\mathbf{U} = [\rho, \rho u_1, \rho u_2, \rho(e + u_1^2/2 + u_2^2/2)]^T$, where u_i is the component of the velocity vector in the direction x_i, for $i = 1, 2$, and e indicates the specific internal energy. The evolution of the conservative variables is finally governed by the 2-D Navier-Stokes equations, as formulated by Marsden et al. (2014) and Sabatini et al. (2016).

At the instant $t = 0\,\mathrm{s}$, the initial undisturbed atmospheric flow, whose variables are marked with an overbar, is defined as a stationary, stratified, and laminar medium, with a wind in the x_1 direction. It is constructed by specifying the vertical profiles of the temperature $\bar{T}(x_2)$ and of the horizontal flow $\bar{u}_1(x_2)$.

Three different configurations are investigated. In the first case, the function $\bar{T}(x_2)$ is defined through the NRLMSISE-00 model (Picone et al., 2002), whereas an HWM profile (Drob et al., 2008) is used for the horizontal flow $\bar{u}_1(x_2)$. The background propagation medium thereby specified is laminar and characterized only by large scales. As an illustration, the speed of sound $\bar{c}(x_2)$ and the wind $\bar{u}_1(x_2)$ are displayed in Figures 1a and 1b, respectively, with regions of the atmosphere identified.

An impulsive sinusoidal IAW is excited into the above initial state at $t = t_{\mathrm{aw}} = 0\,\mathrm{s}$. To this end, as suggested by Sabatini et al. (2016), the following forcing term is added to the right-hand side of the energy equation:

$$\Lambda_{\rho e_t} = \begin{cases} \frac{A_{\rho e_t}}{2} \sin(\omega_{\mathrm{aw}} t^*)\left[1 - \cos(\omega_{\mathrm{aw}} t^*)\right] \exp\left[-\sum_{i=1}^{2} \frac{(x_i - x_{i,\mathrm{aw}})^2}{2\sigma_{i,\mathrm{aw}}^2}\right] & t^* \equiv (t - t_{\mathrm{aw}}) \in [0, T_{\mathrm{aw}}] \\ 0 & \text{otherwise} \end{cases}.$$

The parameter $A_{\rho e_t}$ represents the source amplitude, $\omega_{\mathrm{aw}} = 2\pi/T_{\mathrm{aw}}$ is the angular frequency, $T_{\mathrm{aw}} = 10\,\mathrm{s}$ is the source period, $(x_{1,\mathrm{aw}} = 350\,\mathrm{km}, x_{2,\mathrm{aw}} = 0\,\mathrm{km})$ is the source position, and $\sigma_{1,\mathrm{aw}} = \sigma_{2,\mathrm{aw}} = 600\,\mathrm{m}$ is the source half width.

In the second configuration, before exciting the IAW, a MW is generated into the same initial atmosphere. To this purpose, as proposed by Heale et al. (2017), the following forcing term is introduced in the vertical momentum equation:

$$\Lambda_{\rho u_2} = \rho A_{\rho u_2} \cos(k_{1,\mathrm{mw}}(x_1 - x_{1,\mathrm{mw}})) \exp\left[-\sum_{i=1}^{2} \frac{(x_i - x_{i,\mathrm{mw}})^2}{2\sigma_{i,\mathrm{mw}}^2} - \frac{(t - t_{c,\mathrm{mw}})^2}{2\sigma_{t,\mathrm{mw}}^2}\right].$$

In this formula, $A_{\rho u_2} = 0.1\,\mathrm{m/s}$ is the amplitude, $k_{1,\mathrm{mw}} = 2\pi/(50\,\mathrm{km})$ is the source wavenumber, $(x_{1,\mathrm{mw}} = 450\,\mathrm{km}, x_{2,\mathrm{mw}} = 10\,\mathrm{km})$ is the forcing center in space, $t_{c,\mathrm{mw}} = 8,000\,\mathrm{s}$ is the source center in time, and $\sigma_{1,\mathrm{mw}} = 50\,\mathrm{km}$, $\sigma_{2,\mathrm{mw}} = 3\,\mathrm{km}$, and $\sigma_{t,\mathrm{mw}} = 2,000\,\mathrm{s}$ are the half widths. The breaking of this MW induces small-scale fluctuations into the initial atmosphere. Once a 2-D unsteady turbulent field is developed, at $t = t_{\mathrm{aw}} = 7.84\,\mathrm{hr}$, the impulsive sinusoidal IAW is launched.

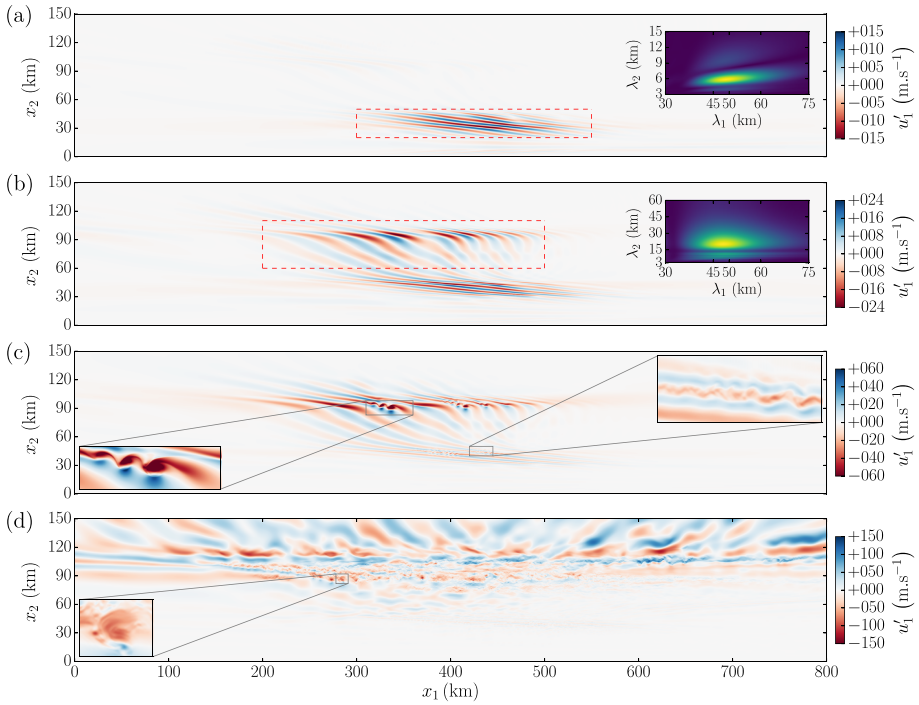

Figure 2. Horizontal velocity perturbations u_1' at four different instants of time: (a) $t = t_1 = 3.92$ hr, (b) $t = t_2 = 4.99$ hr, (c) $t = t_3 = 5.36$ hr, and (d) $t = t_4 = 7.84$ hr. In (a) and (b), the 2-D Fourier transforms of the horizontal velocity fields enclosed by the red boxes are also plotted in the upper-right corners. In (c) and (d), zooms of particular regions of the mountain-wave field are displayed as well.

In the third configuration, the IAW is again excited into a stationary, stratified, and laminar atmosphere. However, in this last case, the temperature $\bar{T}(x_2)$ and the horizontal wind $\bar{u}_1(x_2)$ are extracted at $x_1 = 450$ km and at $t = 7.84$ hr from the 2-D unsteady turbulent MW field. These functions are displayed versus altitude in purple in Figures 1a and 1b and can be seen as the sum of the previous laminar profiles with specific additional fluctuations. The purpose in investigating such a configuration is to analyze whether the effects of the turbulent inhomogeneities can be properly described by adding 1-D stationary small-scale perturbations to 1-D laminar vertical profiles, as it is done in most of the earlier studies.

For the first and the second configurations, simulations are performed with two different amplitudes of the IAW source: $A_{\rho e_t} = 500\,\mathrm{J{\cdot}m^{-3}{\cdot}s^{-1}}$ and $A_{\rho e_t} = 5,000\,\mathrm{J{\cdot}m^{-3}{\cdot}s^{-1}}$. For the third configuration, only a computation is carried out with $A_{\rho e_t} = 5,000\,\mathrm{J{\cdot}m^{-3}{\cdot}s^{-1}}$. The five simulations are labeled as WNL, WNLMW, NL, NLMW, and NLP, where the acronyms WNL and NL are defined for *weakly nonlinear* and *nonlinear*, respectively, and are used to indicate the importance of nonlinearities. Simulations WNL and NL include the acoustic waves alone, at the two amplitudes; cases WNLMW and NLMW include the acoustic waves launched into the MWs, again at the same two amplitudes; and computation NLP involves the nonlinear acoustic wave launched into the 1-D perturbed profiles.

3. Results

3.1. Time Evolution of the MW in the Cases WLMW and NLMW

The horizontal velocity perturbations $u_1' \equiv u_1 - \bar{u}_1$ associated with the MW (i.e., in the cases WNLMW and NLMW) and obtained at $t = t_1 = 3.92$ hr, $t = t_2 = 4.98$ hr, $t = t_3 = 5.36$ hr, and $t = t_4 = 7.84$ hr are illustrated in Figures 2a–2d, respectively, as functions of range and altitude. A video illustrating the evolution in time of the variable u_1' is also provided as Supporting Information S1. In Figures 2a and 2b, the 2-D Fourier transforms of the fields enclosed by the red boxes are additionally plotted in the upper-right corners. In Figures 2c and 2d, zooms of particular flow regions are displayed as well. At $t = t_1$ (cf. Figure 2a), a left-going MW (with negative horizontal wave number k_1) is observed in the stratosphere between 20- and 50-km altitude. The dominant horizontal wavelength $\bar{\lambda}_1$ is about 50 km, whereas the vertical wavelength $\bar{\lambda}_2$ is around 6 km. At $t = t_2$ (cf. Figure 2b), the MW has propagated in the mesosphere and lower thermosphere,

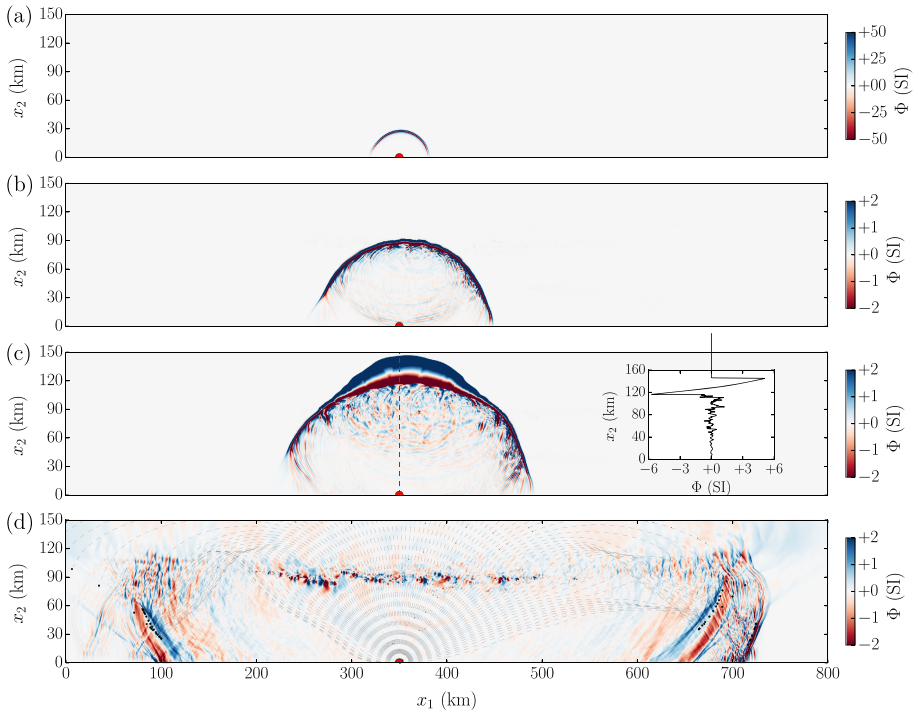

Figure 3. Scaled pressure field Φ at four different instants of time: (a) $t^* = t_5^*$, (b) $t = t_6^*$, (c) $t = t_7^*$, and (d) $t = t_8^*$. In (c), a vertical cut of the variable Φ extracted at $t = t_7^*$ and at $x_1 = 350$-km range is also reported.

where the dominant vertical wavelength $\bar{\lambda}_2$ is of the order of 20 km. At $t = t_3$ (cf. Figure 2c), vortices develop in both the stratosphere (at about $x_2 = 45$-km altitude) and the lower thermosphere (around $x_2 = 90$-km altitude). At $t = t_4$ (cf. Figure 2d), a 2-D turbulent field is observed. The amplitude of the horizontal velocity fluctuations is of about 15 m/s at around $x_2 = 50$-km altitude and can reach values as high as 100 m/s in the lower thermosphere at $x_2 = 125$-km altitude.

3.2. Time Evolution of the IAW in the NLMW Case

The scaled pressure field $\Phi \equiv (p - \bar{p} - p_{\mathrm{mw}})/\sqrt{\bar{\rho}}$ obtained at $t^* \equiv t - t_{\mathrm{aw}} = t_5^* = 93.3$ s, $t^* = t_6^* = 291.7$ s, $t^* = t_7^* = 420$ s, and $t^* = t_7^* = 1,166.7$ s in the NLMW case are illustrated in Figures 3a–3d, respectively, as functions of range and altitude. A video illustrating the evolution in time of the variable Φ is provided as Supporting Information S1. A vertical cut of the function Φ extracted at $x_1 = 350$-km range is also reported in Figure 3c. Note that, in order to only visualize the IAW, the MW field has been subtracted in the function Φ. Moreover, to elucidate the pressure field, the acoustic rays are also depicted in Figure 3d.

Near the source location (cf. Figure 3a), a cylindrical wavefront is observed. However, mainly as a result of the vertical gradients of the speed of sound and of the horizontal wind, the IAW is continuously deformed during its propagation. At the instant $t = t_6^*$ (cf. Figure 3b), partial reflections and scattering are clearly visible in the stratosphere. Moreover, because of nonlinearities, the acoustic wavefront steepens, converts into an N wave (cf. the vertical cut of Φ shown in Figure 3c), and then lengthens while propagating toward the thermosphere. After the instant $t = t_7^*$, the IAW is refracted back toward the Earth's surface. Two arrivals are predicted at large distances at the right of the acoustic source location: a stratospheric return and a thermospheric return. On the contrary, since the wind is globally blowing in the positive x_1 direction, only a thermospheric arrival is observed for $x_1 < x_{1,\mathrm{aw}}$. At the instant $t = t_8^*$, the acoustic wavefront has a complex shape and is a superposition of partial reflections, scattered waves, and stratospheric and thermospheric returns.

3.3. Signals at Ground Level

The signals $\tilde{p} \equiv (p - \bar{p} - p_{\mathrm{mw}})$ obtained from the five simulations at ground level, at $x_1 = x_{1,1} = 0$ km, at $x_1 = x_{1,2} = 650$ km, and at $x_1 = x_{1,3} = 725$ km, are plotted in Figures 4a–4f. In the presence of turbulence, alongside with the main returns (the thermospheric return and eventually the stratospheric

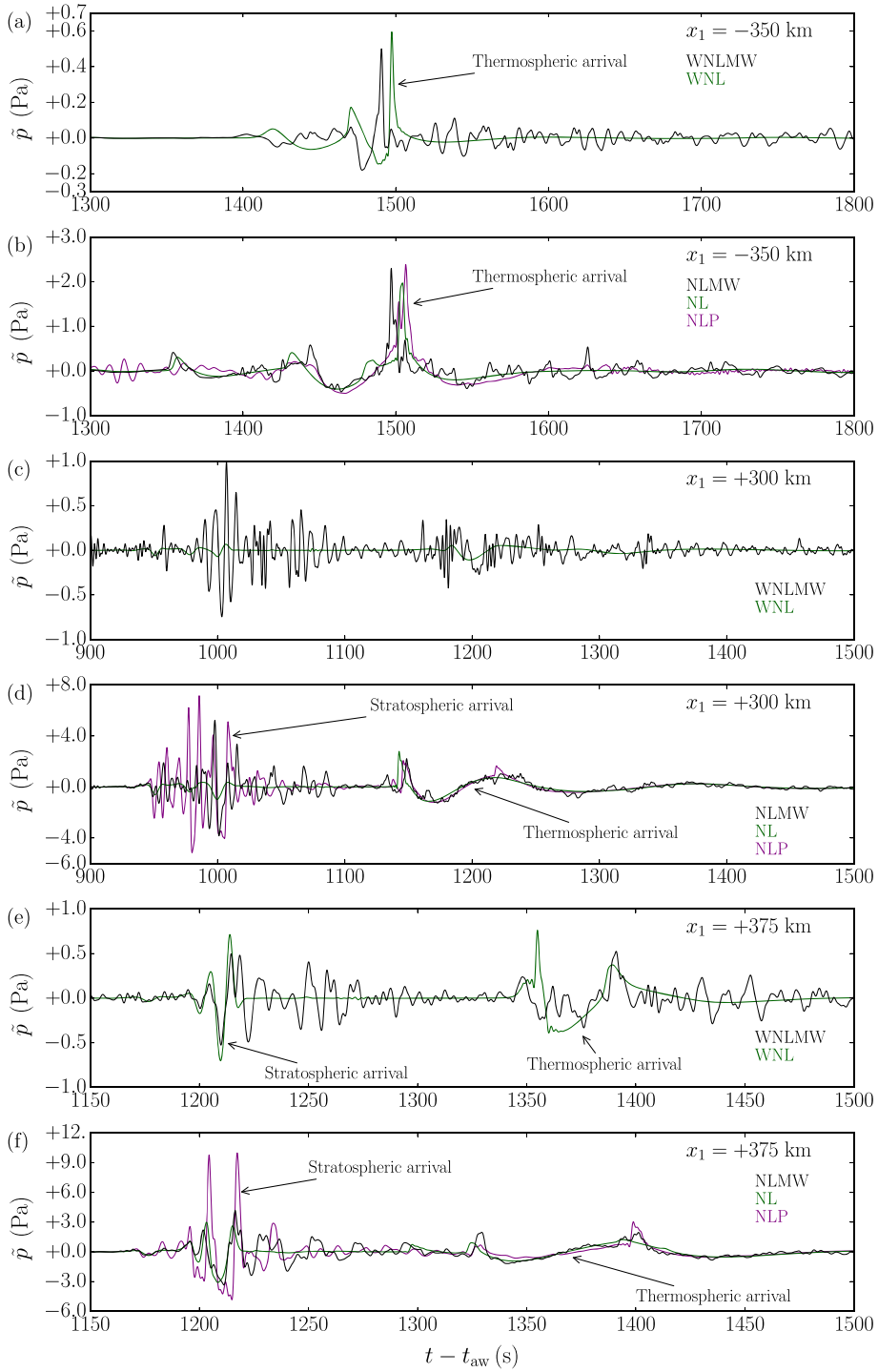

Figure 4. Ground recordings at $x_1 = -350$ km (a, b), $x_1 = +300$ km (c, d), and $x_1 = +375$ km (e, f). The line colors are described in the legends reported in the right sides of the plots.

arrival), a wave train is observed. This latter is generated by scattering and partial reflections, as long as the main wavefront travels through the small-scale atmospheric inhomogeneities. At $x_1 = x_{1,1}$ (cf. Figures 4a and 4b), the thermospheric return exhibits a U-shaped waveform, which is typical of an N wave having crossed a caustic. In both the weakly nonlinear and the nonlinear cases, it is found to be only slightly affected by the small-scale turbulent fluctuations. The thermospheric arrival is also reasonably well predicted by the NLP simulation. Nevertheless, as evident in Figure 4b, the scattered field and the partial reflections are not

reproduced by simply adding stationary 1-D small-scale perturbations to 1-D vertical profiles. At $x_1 = x_{1,2}$, in the geometrical shadow zone, different trends are observed according to the amplitude of the acoustic source. In the weakly nonlinear cases (cf. Figure 4c), both the stratospheric arrival and the thermospheric return are strongly affected by the small-scale atmospheric inhomogeneities. Oppositely, in the NLMW case (cf. Figure 4d), the thermospheric return, which again exhibits a U-shaped waveform, is found to be less sensitive to the GW-induced turbulence. Besides, as at the former recording station, adding stationary 1-D small-scale perturbations to 1-D vertical profiles does not allow recovering the scattered wave packets and the partial reflections. Moreover, the stratospheric arrival recorded in the NLP case exhibits a double U shape which is absent in the NLMW configuration. Finally, at $x_1 = x_{1,3}$, the stratospheric and the thermospheric arrivals are both well reproduced even in the absence of the turbulent field. Once more, adding stationary 1-D small-scale perturbations to 1-D vertical profiles does not correctly recover the scattered train and the partial reflections. Additionally, the amplitude of the stratospheric return obtained in the NLP case is twice higher than that recorded in the presence of turbulence.

4. Discussion and Concluding Remarks

In this work, direct numerical simulations of the 2-D Navier-Stokes equations have been carried out to investigate the interaction between an infrasonic wave and the 2-D turbulent field generated during the early stages of breaking of a MW. The present results demonstrate the feasibility of simulating, within the same code, both the evolution of the GW and turbulent fields and the propagation of the acoustic wave, for the first time in the framework of atmospheric infrasonic acoustics. This study has emphasized infrasonic waves generated at the ground with central frequency of about 0.1 Hz and with wavelength around 3.4 km near the source location; however, the methodology is extendable to a range of smaller and larger scales.

The infrasonic signals recorded at large distances from the source have been presented and described. They consist of a superposition of main returns (in our cases, arrivals of waves following refraction through the thermosphere or stratosphere) and wave packets generated by scattering and partial reflections. The results obtained in this work suggest that, for the frequencies under consideration, the main stratospheric arrivals are more sensitive than the thermospheric ones to the atmospheric small-scale turbulent fluctuations induced by the breaking of MWs. This tendency is particularly evident for strong amplitudes of the acoustic source. The scattered field and the partial reflections are generated when the main acoustic wavefront travels through the atmospheric inhomogeneities. The interaction between the infrasonic wave and these fluctuations depends on both the acoustic wavelength and the length and time scales of the turbulent perturbations (Chunchuzov et al., 2013, 2014; Sabatini et al., 2019), among other factors. As a result, the spectrum of the aforementioned wave packets varies as the amplitude of acoustic source is increased, since the nonlinear lengthening of the main waveform induces an augmentation of the acoustic wavelength impinging on the inhomogeneities.

This investigation also indicates that adding 1-D stationary small-scale fluctuations to 1-D vertical profiles to construct the atmospheric medium, as regularly done in previous studies, does not allow retrieving the scattered field and, in some cases, can strongly and adversely affect both the shape and the amplitude of the main stratospheric return. This suggests that 1-D model atmospheric profiles used for numerical investigations of infrasound propagation should be filtered to include only the variations associated with larger-scale features that can be assumed homogeneous in the horizontal directions.

The present results clearly elucidate the need for an accurate description of the atmospheric small-scale dynamics and turbulence together with the nonlinear infrasonic propagation, in order to compare numerical simulations with observations. In this regard, 3-D simulations of the Navier-Stokes equations are currently envisaged, which will lead to a finer and more quantitative analysis of the interaction between realistic infrasonic waves and GW dynamics and induced fluctuations. Furthermore, this work identifies opportunities to address the influence of the atmospheric dynamics on the IAWs that reach the thermosphere and perturb the ionosphere, which are routinely used as diagnostics of a wide range of geophysical and anthropogenic source processes, such as earthquakes or aboveground and underground explosions.

Acknowledgments
The authors acknowledge support from the Defense Threat Reduction Agency award HDTRA1-16-1-0046 to Purdue University via a subaward to the Embry-Riddle Aeronautical University. The authors also gratefully acknowledge the use of the ERAU Vega High-Performance Computing Cluster and the assistance of Scott Hicks. R. S. and C. B. would also like to thank Olivier Marsden for his precious help in developing the numerical solver and for stimulating discussion. Model outputs generated for this study are too voluminous to retain and are fundamentally theoretical in nature. Thus, detailed movies of the simulations and relevant output fields are provided instead, as supporting information, to enable quantitative comparisons and ensure reproducibility.

References

Assink, J. D., Averbuch, G., Smets, P. S. M., & Evers, L. G. (2016). On the infrasound detected from the 2013 and 2016 DPRK's underground nuclear tests. *Geophysical Research Letters*, *43*, 3526–3533. https://doi.org/10.1002/2016GL068497

Assink, J. D., Evers, L. G., Holleman, I., & Paulssen, H. (2008). Characterization of infrasound from lightning. *Geophysical Research Letters*, *35*, L15802. https://doi.org/10.1029/2008GL034193

Bertin, M., Millet, C., & Bouche, D. (2014). A low-order reduced model for the long range propagation of infrasounds in the atmosphere. *The Journal of the Acoustical Society of America*, *136*(1), 37–52. https://doi.org/10.1121/1.4883388

Bossert, K., Fritts, D. C., Pautet, P.-D., Williams, B. P., Taylor, M. J., Kaifler, B., et al. (2015). Momentum flux estimates accompanying multiscale gravity waves over Mount Cook, New Zealand, on 13 July 2014 during the DEEPWAVE campaign. *Journal of Geophysical Research: Atmospheres*, *120*, 9323–9337. https://doi.org/10.1002/2015JD023197

Bowman, D. C., & Lees, J. M. (2015). Infrasound in the middle stratosphere measured with a free-flying acoustic array. *Geophysical Research Letters*, *42*, 10,010–10,017. https://doi.org/10.1002/2015GL066570

Ceranna, L., Le Pichon, A., Green, D. N., & Mialle, P. (2009). The buncefield explosion: A benchmark for infrasound analysis across Central Europe. *Geophysical Journal International*, *177*(2), 491–508. https://doi.org/10.1111/j.1365-246X.2008.03998.x

Chunchuzov, I. P. (2009). On the nonlinear shaping mechanism for gravity wave spectrum in the atmosphere. *Annales Geophysicae*, *27*(11), 4105–4124. https://doi.org/10.5194/angeo-27-4105-2009

Chunchuzov, I. P., Kulichkov, S. N., & Firstov, P. P. (2013). On acoustic N-wave reflections from atmospheric layered inhomogeneities. *Izvestiya, Atmospheric and Oceanic Physics*, *49*(3), 258–270. https://doi.org/10.1134/S0001433813020060

Chunchuzov, I., Kulichkov, S., Popov, O., & Hedlin, M. (2014). Modeling propagation of infrasound signals observed by a dense seismic network. *The Journal of the Acoustical Society of America*, *135*(1), 38–48. https://doi.org/10.1121/1.4845355

Chunchuzov, I. P., Kulichkov, S. N., Popov, O. E., Perepelkin, V. G., Vasil'ev, A. P., Glushkov, A. I., & Firstov, P. P. (2015). Characteristics of a fine vertical wind-field structure in the stratosphere and lower thermosphere according to infrasonic signals in the zone of acoustic shadow. *Izvestiya, Atmospheric and Oceanic Physics*, *51*(1), 57–74. https://doi.org/10.1134/S0001433814060061

Chunchuzov, I. P., Kulichkov, S. N., Popov, O. E., Waxler, R., & Assink, J. (2011). Infrasound scattering from atmospheric anisotropic inhomogeneities. *Izvestiya, Atmospheric and Oceanic Physics*, *47*(5), 540. https://doi.org/10.1134/S0001433811050045

de Groot-Hedlin, C. D. (2012). Nonlinear synthesis of infrasound propagation through an inhomogeneous, absorbing atmosphere. *The Journal of the Acoustical Society of America*, *132*(2), 646–656. https://doi.org/10.1121/1.4731468

de Groot-Hedlin, C. D. (2016). Long-range propagation of nonlinear infrasound waves through an absorbing atmosphere. *The Journal of the Acoustical Society of America*, *139*(4), 1565–1577. https://doi.org/10.1121/1.4944759

de Groot-Hedlin, C. D. (2017). Infrasound propagation in tropospheric ducts and acoustic shadow zones. *The Journal of the Acoustical Society of America*, *142*(4), 1816–1827. https://doi.org/10.1121/1.5005889

de Larquier, S., Pasko, V. P., Stenbaek-Nielsen, H. C., Wilson, C. R., & Olson, J. V. (2010). Finite-difference time-domain modeling of infrasound from pulsating auroras and comparison with recent observations. *Geophysical Research Letters*, *37*, L06804. https://doi.org/10.1029/2009GL042124

Drob, D. P., Broutman, D., Hedlin, M. A., Winslow, N. W., & Gibson, R. G. (2013). A method for specifying atmospheric gravity wavefields for long-range infrasound propagation calculations. *Journal of Geophysical Research: Atmospheres*, *118*, 3933–3943. https://doi.org/10.1029/2012JD018077

Drob, D. P., Emmert, J. T., Crowley, G., Picone, J. M., Shepherd, G. G., Skinner, W., et al. (2008). An empirical model of the Earth's horizontal wind fields: HWM07. *Journal of Geophysical Research*, *113*, A12304. https://doi.org/10.1029/2008JA013668

Drob, D. P., Picone, J. M., & Garcés, M. (2003). Global morphology of infrasound propagation. *Journal of Geophysical Research*, *108*(D21), 4680. https://doi.org/10.1029/2002JD003307

Fritts, D. C., & Alexander, M. J. (2003). Gravity wave dynamics and effects in the middle atmosphere. *Reviews of Geophysics*, *41*(1), 1003. https://doi.org/10.1029/2001RG000106

Fritts, D. C., Vosper, S. B., Williams, B. P., Bossert, K., Plane, JohnM. C., Taylor, M. J., et al. (2018). Large-amplitude mountain waves in the mesosphere accompanying weak cross-mountain flow during DEEPWAVE research flight RF22. *Journal of Geophysical Research: Atmospheres*, *123*, 9992–10,022. https://doi.org/10.1029/2017JD028250

Gainville, O., Henneton, M., & Coulouvrat, F. (2017). A re-analysis of Carancas meteorite seismic and infrasound data based on sonic boom hypothesis. *Geophysical Journal International*, *209*(3), 1913–1923. https://doi.org/10.1093/gji/ggx122

Gardner, C. S. (1994). Diffusive filtering theory of gravity wave spectra in the atmosphere. *Journal of Geophysical Research*, *99*(D10), 20,601–20,622. https://doi.org/10.1029/94JD00819

Heale, C. J., Bossert, K., Snively, J. B., Fritts, D. C., Pautet, P.-D., & Taylor, M. J. (2017). Numerical modeling of a multiscale gravity wave event and its airglow signatures over Mount Cook, New Zealand, during the DEEPWAVE campaign. *Journal of Geophysical Research: Atmospheres*, *122*, 846–860. https://doi.org/10.1002/2016JD025700

Hecht, J. H., Walterscheid, R. L., Fritts, D. C., Isler, J. R., Senft, D. C., Gardner, C. S., & Franke, S. J. (1997). Wave breaking signatures in OH airglow and sodium densities and temperatures: 1. Airglow imaging, Na lidar, and MF radar observations. *Journal of Geophysical Research*, *102*(D6), 6655–6668. https://doi.org/10.1029/96JD02619

Hedlin, MichaelA. H., & Drob, D. P. (2014). Statistical characterization of atmospheric gravity waves by seismoacoustic observations. *Journal of Geophysical Research: Atmospheres*, *119*, 5345–5363. https://doi.org/10.1002/2013JD021304

Hickey, M. P., Schubert, G., & Walterscheid, R. L. (2001). Acoustic wave heating of the thermosphere. *Journal of Geophysical Research*, *106*(A10), 21,543–21,548. https://doi.org/10.1029/2001JA000036

Kulichkov, S. (2009). On the prospects for acoustic sounding of the fine structure of the middle atmosphere. In A. Le Pichon, E. Blanc, & A. Hauchecorne (Eds.), *Infrasound monitoring for atmospheric studies* (pp. 511–540). Dordrecht, Netherlands: Springer. https://doi.org/10.1007/978-1-4020-9508-516

Lalande, J.-M., & Waxler, R. (2016). The interaction between infrasonic waves and gravity wave perturbations: Application to observations using UTTR rocket motor fuel elimination events. *Journal of Geophysical Research: Atmospheres*, *121*, 5585–5600. https://doi.org/10.1002/2015JD024527

Le Pichon, A., Blanc, E., & Hauchecorne, A. (Eds.) (2009). *Infrasound monitoring for atmospheric studies*. Netherlands: Springer. https://doi.org/10.1007/978-1-4020-9508-5

Le Pichon, A., Garcés, M., Blanc, E., Barthélémy, M., & Drob, D. P. (2002). Acoustic propagation and atmosphere characteristics derived from infrasonic waves generated by the Concorde. *The Journal of the Acoustical Society of America*, *111*(1), 629–641. https://doi.org/10.1121/1.1404434

Luquet, D., Marchiano, R., Coulouvrat, F., Salah El Din, I., & Loseille, A. (2015). Sonic boom assessment of a hypersonic transport vehicle with advanced numerical methods, *AIAA Aviation forum* (pp. 1–13). Dallas, TX: American Institute of Aeronautics and Astronautics. https://doi.org/10.2514/6.2015-2685

Marsden, O., Bogey, C., & Bailly, C. (2014). A study of infrasound propagation based on high-order finite difference solutions of the Navier-Stokes equations. *The Journal of the Acoustical Society of America*, *135*(3), 1083–1095. https://doi.org/10.1121/1.4864793

Matoza, R. S., Fee, D., Garcés, M. A., Seiner, J. M., Ramón, P. A., & Hedlin, M. A. H. (2009). Infrasonic jet noise from volcanic eruptions. *Geophysical Research Letters*, *36*, L08303. https://doi.org/10.1029/2008GL036486

McKisic, J. M. (1997). Infrasound and the infrasonic monitoring of atmospheric nuclear explosions: A literature review.

Mutschlecner, J. P., & Whitaker, R. W. (2005). Infrasound from earthquakes. *Journal of Geophysical Research*, *110*, D01108. https://doi.org/10.1029/2004JD0050067

Norris, D., Gibson, R., & Bongiovanni, K. (2009). Numerical methods to model infrasonic propagation through realistic specifications of the atmosphere. In A. Le Pichon, E. Blanc, & A. Hauchecorne (Eds.), *Infrasound monitoring for atmospheric studies* (pp. 541–573). Dordrecht, Netherlands: Springer. https://doi.org/10.1007/978-1-4020-9508-517

Ostashev, V., & Wilson, D. (2016). *Acoustics in moving inhomogeneous media*. London: CRC Press.

Picone, J. M., Hedin, A. E., Drob, D. P., & Aikin, A. C. (2002). NRLMSISE-00 empirical model of the atmosphere: Statistical comparisons and scientific issues. *Journal of Geophysical Research*, *107*(A12), 1468. https://doi.org/10.1029/2002JA009430

Sabatini, R., Marsden, O., Bailly, C., & Bogey, C. (2016). A numerical study of nonlinear infrasound propagation in a windy atmosphere. *The Journal of the Acoustical Society of America*, *140*(1), 641–656. https://doi.org/10.1121/1.4958998

Sabatini, R., Marsden, O., Bailly, C., & Gainville, O. (2019). Three-dimensional direct numerical simulation of infrasound propagation in the Earth's atmosphere. *Journal of Fluid Mechanics*, *859*, 754–789. https://doi.org/10.1017/jfm.2018.816

Snively, J. B., & Pasko, V. P. (2008). Excitation of ducted gravity waves in the lower thermosphere by tropospheric sources. *Journal of Geophysical Research*, *113*, A06303. https://doi.org/10.1029/2007JA012693

Tsuda, T. (2014). Characteristics of atmospheric gravity waves observed using the MU (Middle and Upper atmosphere) radar and GPS (Global Positioning System) radio occultation. *Proceedings of the Japan Academy, Series B Physical and Biological Sciences*, *90*, 12–27. https://doi.org/10.2183/pjab.90.12

Walterscheid, R. L., & Hickey, M. P. (2005). Acoustic waves generated by gusty flow over hilly terrain. *Journal of Geophysical Research*, *110*, A10307. https://doi.org/10.1029/2005JA011166

Yang, Y.-M., Garrison, J. L., & Lee, S.-C. (2012). Ionospheric disturbances observed coincident with the 2006 and 2009 North Korean underground nuclear tests. *Geophysical Research Letters*, *39*, L02103. https://doi.org/10.1029/2011GL050428

Zettergren, M. D., & Snively, J. B. (2015). Ionospheric response to infrasonic-acoustic waves generated by natural hazard events. *Journal of Geophysical Research: Space Physics*, *120*, 8002–8024. https://doi.org/10.1002/2015JA021116

Zettergren, M. D., & Snively, J. B. (2019). Latitude and longitude dependence of ionospheric tec and magnetic perturbations from infrasonic-acoustic waves generated by strong seismic events. *Geophysical Research Letters*, *46*, 1132–1140. https://doi.org/10.1029/2018GL081569